INTERNATIONAL SOCIETY FOR SOIL MECHANICS AND GEOTECHNICAL ENGINEERING



This paper was downloaded from the Online Library of the International Society for Soil Mechanics and Geotechnical Engineering (ISSMGE). The library is available here:

https://www.issmge.org/publications/online-library

This is an open-access database that archives thousands of papers published under the Auspices of the ISSMGE and maintained by the Innovation and Development Committee of ISSMGE.

Investigating the Mechanical Underpinnings of Origin of Liquefaction in Field

U. Mital¹, J.E. Andrade², T. Mohammadnejad³

ABSTRACT

The state-of-the-practice uses the "simplified procedure" to evaluate the liquefaction resistance of soils. This procedure involves estimating the stresses induced during a design earthquake at a given site, and comparing them with the stresses required to liquefy the in-situ soil. Determination of stresses required to liquefy the in-situ soil is a largely empirical process that is based on field data obtained from past earthquakes, requiring an engineer to exercise considerable judgment. Our objective is to make this particular evaluation more deterministic. We numerically simulate the lower end of liquefaction curves. Liquefaction is flagged using a physics-based criterion. The curve obtained using this criterion agrees closely with the curve in literature. Hence, the use of such a criterion may enable an engineer to make more sophisticated estimates while evaluating liquefaction susceptibility at a site.

Introduction

The state-of-the-practice uses the "simplified procedure" (Seed & Idriss, 1971) for evaluating liquefaction susceptibility of soils. The procedure involves estimating the stresses induced during a design earthquake at a given site, and comparing them with the stresses required to induce liquefaction in the in-situ soil. Determination of these stresses is a largely empirical process and often requires an engineer to exercise considerable judgment. Soil testing for evaluating liquefaction susceptibility can be done in the lab or in the field. Presently, it is more usual to rely on field tests, common among which are the standard penetration test (SPT), the cone penetration test (CPT), and shear-wave velocity measurements (V_S). Such tests have also been extensively used to collect case histories that have aided in the development of liquefaction charts to assess liquefaction susceptibility at a site.

To get the most out of field data and to make liquefaction susceptibility a more deterministic process, it is vital that research be carried out to incorporate more physics in this evaluation. As pointed out by Idriss & Boulanger (2004), incorporating physics helps make more sense out of laboratory or field data and gives us more confidence when it comes to evaluating liquefaction potential in light of insufficient data. Studies have been conducted in the past (for instance, Vaid & Chern, 1983; Idriss & Boulanger, 2004; Dobry & Abdoun, 2011) to bridge the gap between physics and empiricism. This paper seeks to take another step in that direction.

We start by making two observations from literature, which we find to be pertinent to the work presented in this paper. Firstly, regardless of the liquefaction index used, liquefaction charts are quite similar qualitatively (Idriss & Boulanger, 2008). This makes sense since indices such as relative density, SPT count, CPT tip resistance and shear-wave velocity seem

¹Graduate Student, Applied Mechanics, California Institute of Technology, Pasadena, USA, <u>umital@caltech.edu</u>
²Professor, Civil and Mechanical Engineering, California Institute of Technology, Pasadena, USA, <u>jandrade@caltech.edu</u>

³Post Doctoral Scholar, Mechanical and Civil Engineering, California Institute of Technology, Pasadena, USA, toktam@caltech.edu

to be directly correlated to each other (Gibbs & Holtz, 1957; Marcuson & Bieganousky, 1977; Ohta & Goto, 1978; Schmertmann, 1979). Hence, a deeper understanding of the influence of any one index on liquefaction resistance could assist in a better understanding of the influence of other indices. Secondly, we refer to the work by Dobry & Abdoun (2011), which concludes that liquefaction charts essentially constitute curves of constant cyclic shear strain. A soil subjected to strains higher than those corresponding to the liquefaction curves will liquefy. At the lower end of these curves, the cyclic strain is only slightly larger than the threshold strain, which is the amount of strain below which sand does not develop any pore pressure. The upper end of these curves corresponds to increasingly high values of cyclic strain, and is likely controlled by overconsolidated and preshaken sands.

In this paper, we numerically simulate the lower end of liquefaction resistance curve as a function of relative density. In our simulations, liquefaction is flagged using a physics-based criterion. The liquefaction curve that we obtain is comparable to the lower end of the liquefaction curve obtained by Seed & Peacock (1970). This suggests that there may be merit in using the physics-based criterion to assess liquefaction susceptibility. It will soon become apparent that our work complements recent work by Dobry & Abdoun (2011). This could take us closer to integrating the states of the art and practice for evaluating liquefaction susceptibility.

Flow Liquefaction and Cyclic Mobility

We start by presenting a formal classification of liquefaction into flow liquefaction and cyclic mobility (National Research Council, 1985). Flow liquefaction (Figure 1) refers to "the condition where a soil mass can deform continuously under shear stress less than or equal to the static shear stress applied to it." This initiates as an instability with rapid rise in pore pressure and is associated with loss of strength. Examples include slope instability and bearing capacity failures. Onset of instability leading to flow liquefaction is initiated at small values of strain (Kramer, 1996), suggesting that flow liquefaction corresponds to the lower end of the curve in liquefaction charts.

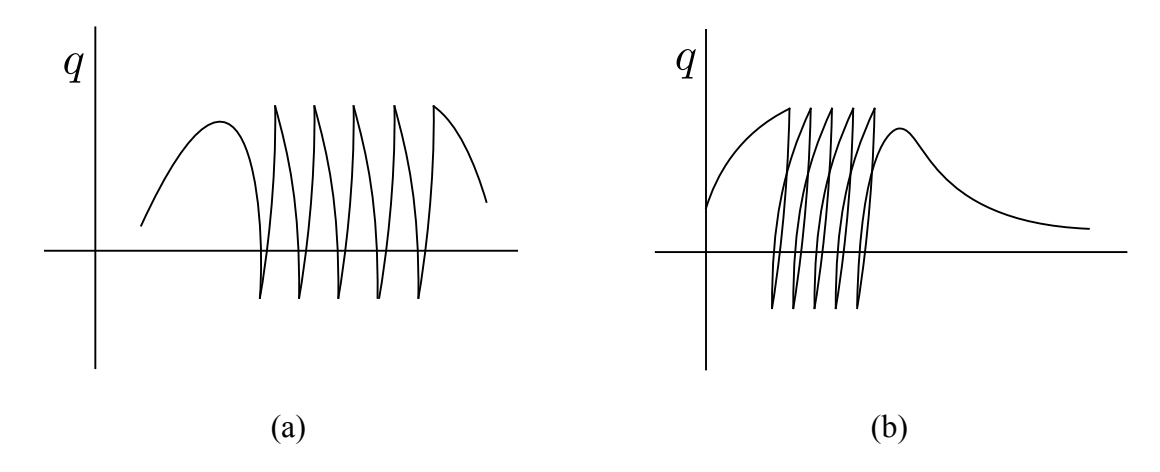


Figure 1. Schematic for flow liquefaction during cyclic loading; (a) deviatoric stress (q) vs effective pressure (p'); (b) deviatoric stress (q) vs shear strain (ϵ_s)

On the other hand, cyclic mobility (Figure 2) refers to (National Research Council, 1985) "unacceptable large permanent displacements or settlements during shaking, but earth mass remains stable following shaking without great changes in geometry." Examples of cyclic mobility are settlements of oil tanks and slumping and cracking of earth dams. Cyclic

mobility can occur in both normally and over consolidated deposits and does not have a clear initiation point. In addition, pore pressure build up is also less intense. This suggests that cyclic mobility may correspond to the upper end of the curve in liquefaction charts.

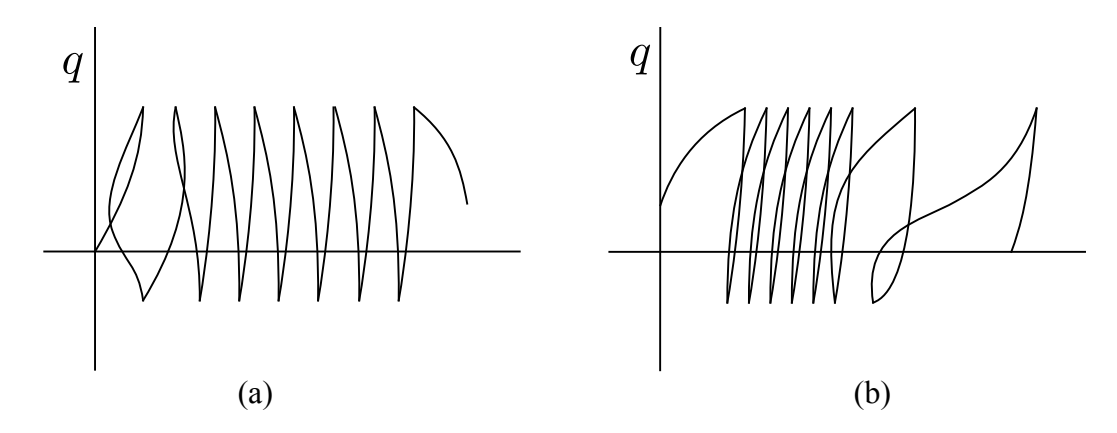


Figure 2. Schematic for cyclic mobility during cyclic loading; (a) deviatoric stress (q) vs effective pressure (p'); (b) deviatoric stress (q) vs shear strain (ϵ_s)

In this work, we focus our attention on flow liquefaction, since we are interested in the lower end of liquefaction curves.

Hill's Criterion for Loss of Stability

Hill's criterion (Hill, 1975) is a physics-based criterion that can be used to predict the onset of flow liquefaction (Lade, 1992; Andrade, 2009). According to Hill's criterion, loss of stability for an undrained cyclic triaxial test can be expressed as:

$$\dot{q}\dot{\epsilon_s} \le 0 \tag{1}$$

where \dot{q} is the increment in deviatoric stress and $\dot{\epsilon}_s$ is the increment in shear strain. If $\dot{\epsilon}_s > 0$ (compressive loading), then instability will occur if $\dot{q} \leq 0$. This implies that under compressive loading, instability leading to flow liquefaction is initiated when the stress path peaks, and the soil sample is unable to sustain the imposed shear stresses (as shown in Figure 1). This is consistent with experimental observations (Castro, 1969; Vaid & Chern, 1983).

Simulations of Undrained Cyclic Triaxial Test

For the purpose of our simulations, we used the Dafalias-Manzari plasticity model (Dafalias & Manzari, 2004), as implemented by Mohammadnejad & Andrade (2015). We calibrated the model to some experiments carried out by Vaid & Chern (1983). Table 1 in appendix outlines the parameters used in the model. Figure 3 shows a calibration test corresponding to a stress-controlled, undrained cyclic loading experiment. The simulation captures two important aspects of the experiment. Firstly, flow liquefaction initiates following a peak in the stress path, which occurs in the 8th cycle. Secondly, the cyclic stress ratio (CSR), i.e., the ratio between the *imposed* deviatoric stress and the *initial* confining pressure is the same in both experiment and simulation.

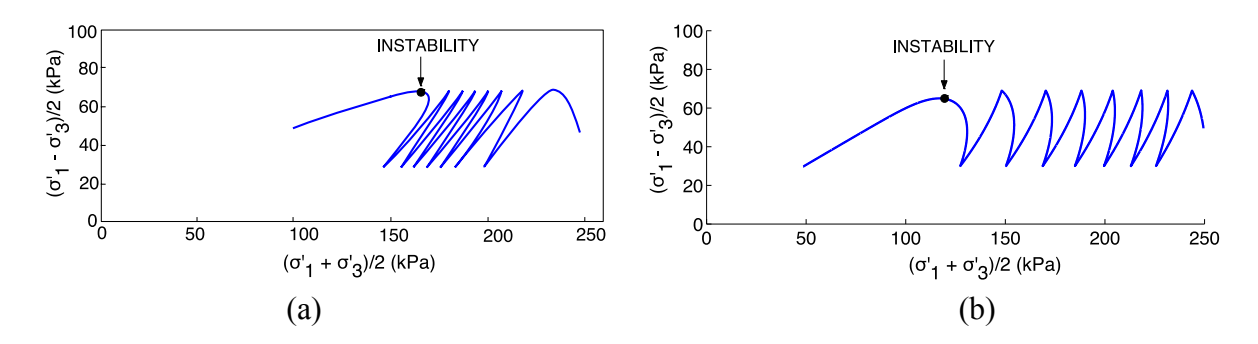


Figure 3. Calibration of the model (σ'_1 and σ'_3 are the major and minor effective principal stresses, respectively); (a) Experiment; (b) Simulation

Simulating the Lower End of Liquefaction Curve

In order to simulate the lower end of the liquefaction resistance curve as a function of relative density, we picked relative densities over a fairly narrow range of 31% - 42%. The lower limit of relative density is in accordance with the lower limit considered by Vaid & Chern (1983). Each sample had an initial pressure of 100 kPa and a static shear stress of 75 kPa, yielding $K_0 = 0.5$. This initial state ensured that the soil was susceptible to flow liquefaction over the range of relative densities considered. Each sample was subjected to 10 loading cycles under undrained triaxial conditions. Flow liquefaction instability was deemed to have occurred in accordance with Hill's criterion, that is, when the stress path peaked. Cyclic stress ratio (CSR) that caused instability in the 10^{th} cycle was recorded as the cyclic resistance ratio (CRR). Figure 4(a) shows the liquefaction curve that we obtain using this method. We can see from Figure 4(b) that our curve resembles the lower end of the liquefaction curve as proposed by Seed & Peacock (1970).

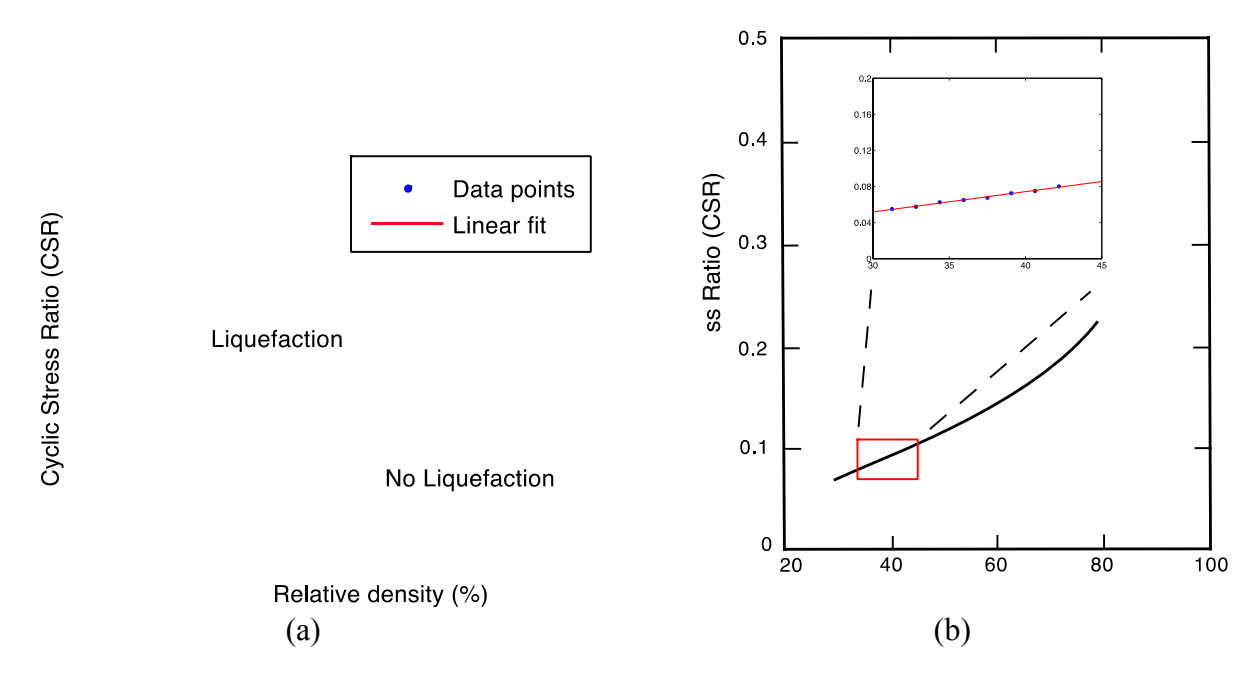


Figure 4. Liquefaction curves as a function of relative density; (a) curve obtained using our simulations; (b) comparison with lower end of the Seed & Peacock (1970) curve.

Conclusions

We have used Hill's criterion, which is a physics-based criterion, to simulate the lower end of the liquefaction curve as a function of relative density. This suggests that soil samples corresponding to the lower end of liquefaction curves are susceptible to flow liquefaction, which initiates as an instability at small strains and is accompanied with rapid build up of pore pressure. Hence, the use of Hill's criterion may enable an engineer to make more sophisticated estimates of liquefaction susceptibility at a site. This complements a conclusion put forward by Dobry & Abdoun (2011), that the lower end of liquefaction curves represent soil samples that liquefy under small strains. Work is currently underway on simulating correction factors for overburden stress and static shear, for soil samples corresponding to the lower end of liquefaction curves. The preliminary results look promising and will be discussed in a subsequent publication. This could arm us with a better understanding of the mechanical underpinnings of liquefaction not only in the lab, but also in the field.

References

Andrade JE. A predictive framework for liquefaction instability. Geotechnique 2009; 59 (8): 673-682.

Castro G. Liquefaction of Sands. PhD Thesis, Harvard University, Department of Civil Engineering, 1969

Dafalias YF, Manzari MT. Simple plasticity sand model accounting for fabric change effects. Journal of Engineering Mechanics 2004; 130 (6): 622-634.

Dobry R, Abdoun T. An investigation into why liquefaction charts work: A necessary step towards integrating the states of art and practice. *5th International Conference on Earthquake Geotechnical Engineering* 2011; 13-45.

Gibbs HJ, Holtz WG. Research on determining the density of sand by spoon penetration test. *Fourth International Conference on Soil Mechanics and Foundations Engineering* 1957; 35-39.

Hill R. Elasticity and stability of perfect crystals at finite strain. *Mathematical Proceedings of the Cambridge Philosophical Society* 1975; 77 (1): 225-240.

Idriss IM, Boulanger RW. Semi-empirical procedures for evaluating liquefaction potential during earthquakes. *Soil Dynamics and Earthquake Engineering* 2004; **26** (2): 115-130.

Idriss IM, Boulanger RW. Soil liquefaction during earthquakes. Earthquake Engineering Research Institute, 2008.

Kramer SL. Geotechnical earthquake engineering. Prentice Hall: Upper Saddle River, New Jersey, 1996.

Lade PV. Static instability and liquefaction of loose fine sandly slopes. *Journal of Geotechnical Engineering* 1992; **118** (1): 51-71.

Marcuson WF, Bieganousky WA. Laboratory standard penetration tests on fine sands. *Journal of the Geotechnical Engineering Division* 1977; **103** (6): 565-588.

Mohammadnejad T, Andrade JE. Flow liquefaction instability prediction using finite elements. *Acta Geotechnica* 2015; **10**: 83-100.

National Research Council. *Liquefaction of soils during earthquakes*. National Academy Press: Washington, DC, 1985.

Ohta Y, Goto N. Empirical shear wave velocity equations in terms of characteristic soil indexes. *Earthquake Engineering & Structural Dynamics* 197; **6** (2): 167-187.

Schmertmann JH. Statics of SPT. Journal of the Geotechnical Engineering Division 1979; 105 (5): 655-670.

Seed HB, Idriss IM. Simplified procedure for evaluating soil liquefaction potential. Journal of Soil Mechanics & Foundations Div 1971; **97** (9): 1249-1273.

Seed HB, Peacock WH. Applicability of laboratory test procedures for measuring soil liquefaction characteristics under cyclic loading. Earthquake Engineering Research Center, 1970.

Vaid YP, Chern JC. Effect of static shear on resistance to liquefaction. Soils and Foundations 1983; 23(1): 47-60

Appendix

Table 1. Parameters for the Dafalias-Manzari constitutive model

Constant	Variable	Value
Elasticity	G_0	125
	ν	0.05
Critical State	M	1.45
	λ_c	0.065
	e_0	0.722
	$e_0 \ oldsymbol{\xi}$	0.9
Yield surface	m	0.01
Plastic modulus	h_0	4.5
	c_h	1.05
	n^b	1.1
Dilatancy	A_0	0.124
	$n^{\check{d}}$	5.5
Fabric-dilatancy tensor	$z_{ m max}$	4
	C_Z	600